The Cryosphere Discuss., 8, 4885–4912, 2014
www.the-cryosphere-discuss.net/8/4885/2014/
doi:10.5194/tcd-8-4885-2014

The Cryosphere Discussions Open Access

Interaction of marine ice-sheet instabilities in two drainage basins: simple scaling of geometry and transition time

J. Feldmann[1,2] **and A. Levermann**[1,2]

[1]Potsdam Institute for Climate Impact Research (PIK), Potsdam, Germany
[2]Institute of Physics, University of Potsdam, Potsdam, Germany

Received: 15 August 2014 – Accepted: 1 September 2014 – Published: 12 September 2014

Correspondence to: J. Feldmann (johannes.feldmann@pik-potsdam.de)

Published by Copernicus Publications on behalf of the European Geosciences Union.

Abstract

Recent regional simulations and observations suggest a destabilization of the Amundsen Sea sector of West Antarctica. Whether the initiated ice drainage will be limited to Pine Island and Thwaites basin or extend to the Filchner–Ronne basin depends on the possibility of an interaction of the different drainage basins. Using a conceptional flow-line geometry, we investigate the possibility of whether a marine ice-sheet instability (MISI) can be triggered from the direction of the ice divide as opposed to coastal forcing and investigate the interaction between connected basins. We find that the initiation of a MISI in one basin can induce a destabilization in the other. The underlying mechanism of basin interaction is based on dynamic thinning and a consecutive motion of the ice divide which induces a thinning in the adjacent basin and a successive initiation of the instability. Our simplified and symmetric topographic set-up allows to scale both the geometry and the transition time between both instabilities. We find that the ice profile follows a universal shape that is scaled with the horizontal extent of the ice sheet and that the same exponent of 1/2 applies for the scaling relation between central surface elevation and horizontal extent as in the pure Shallow Ice Approximation (Vialov profile). Altering the central bed elevation we find that the extent of grounding line retreat in one basin determines the degree of interaction with the other. We conclude that for the three-dimensional case the possibility of such drainage basin interaction cannot be excluded and hence needs further investigation.

1 Introduction

Recent studies that investigate the future evolution of the West Antarctic Ice Sheet (WAIS) by basin-scale numerical modeling suggest that a destabilization of parts of it is under way (Katz and Worster, 2010; Favier et al., 2014; Joughin et al., 2014). The bed geometry of the WAIS (Figs. 1 and 2) makes it susceptible to a marine ice-sheet instability (MISI), proposed several decades ago (Mercer, 1978; Schoof, 2007; Joughin and Alley, 2011). Pine Island Glacier (PIG) and Thwaites Glacier (TG) are two major tributaries of the WAIS, are most likely out-of-balance and exhibit the highest single-glacier mass loss in Antarctica (Rignot et al., 2008; Medley et al., 2014). Among other smaller glaciers in the Amundsen Sea sector they show a grounding line retreat on retrograde (inland down-sloping) bed sections (Fig. 2) that reach deep into the interior of their basins (Vaughan et al., 2006; Tinto and Bell, 2011). The lack of substantial bed obstacles along these sections indicates that observed rapid changes, including grounding line retreat, ice acceleration and thinning (Shepherd et al., 2002; Pritchard et al., 2012; Park et al., 2013; Mouginot et al., 2014), and thus destabilization are likely to continue (Rignot and Mouginot, 2014). The changes are attributed to increased sub-ice-shelf melting that is driven by relatively warm circumpolar deep water reaching towards the glaciers' grounding lines (Walker et al., 2007; Jacobs et al., 2011; Rignot et al., 2013). PIG and TG basins contain enough ice to raise global sea level by ~ 24 cm and ~ 59 cm, respectively (Holt et al., 2006; Vaughan et al., 2006).

It can be presumed that a full drainage of one of these basins or of both basins would imply an even larger sea-level contribution due to additional ice supply from other connected basins (Stuiver et al., 1981; Holt et al., 2006). Multiple studies show that due to ice stream thinning, marginal (grounding line) retreat or changing accumulation patterns ice divides can indeed shift (Anandakrishnan et al., 1994; Cuffey and Clow, 1997; Nereson et al., 1998). Prominent examples are Siple Dome and two other inter-ice-stream ridges in West Antarctica whose ice divides have migrated in response to changed dynamics in their lateral ice streams (Nereson and Raymond, 2001). Numerical modeling of the response of the Antarctic Ice Sheet to extensive sub-ice-shelf melting (SeaRISE project, Bindschadler et al., 2013) showed the possibility of a collapse of the WAIS that implies the migration of ice divides and the eventual merging of several drainage basins in West Antarctica. However, in the SeaRISE experiments the coastal forcing was applied to the whole Antarctic Ice Sheet and hence all drainage basins where perturbed simultaneously. With this approach no statements can be made on the influence of a perturbed basin on a connected unperturbed basin.

TCD
8, 4885–4912, 2014

Here we investigate how the ice dynamics in a drainage basin can be affected by changes originating from the direction of the ice divide as opposed to coastal forcing and analyze the interaction between connected basins. Using a flow-line setup, we show that the initiation of a MISI in one basin leads to grounding line retreat in a connected basin and can trigger its destabilization. First of all we describe our symmetric model setup and the set of experiments, designed to perturb a steady-state ice sheet. We then analyze the evolution of the relaxing ice sheet in response to the perturbation. A simple scaling of the steady-state ice surface elevation as well as the transition time between the instabilities in both basins is proposed. Finally, we discuss the results and conclude.

2 Model and experiments

The model we use in our experiments is the Parallel Ice Sheet Model (PISM). It is an open-source, thermo-mechanically coupled, three-dimensional model (Bueler and Brown, 2009, http://www.pism-docs.org). PISM uses a superposition of the shallow ice and the shallow shelf approximations (SIA and SSA) of the stress balance to calculate ice velocities (Winkelmann et al., 2011). Since the SSA velocities are used as basal velocities for the grounded parts of the ice, a smooth transition of the velocity field between the grounded and floating regimes is ensured (Martin et al., 2011). The model used in this study is based on PISM version stable0.5. The combination of (1) a linear interpolation of the grounding line with locally interpolated basal friction and (2) a modified driving-stress computation across the grounding line led to a significantly improved performance of PISM in MISMIP3d (shown in Feldmann et al., 2014, compare to Pattyn et al., 2013). For the experiments in the present study sub-ice-shelf melt rates are parameterized following Beckmann and Goosse (2003). Here, melt rates are proportional to the temperature difference between a prescribed value for the water in the sub-shelf cavity and the local pressure melting point of the ice.

The computational domain of our setup stretches from −800 to 800 km in x direction (flow direction). The bed geometry (Fig. 3, black line) is symmetric around $x_c = 0$ and is similar to a bed geometry introduced by Schoof (2007), which was later used in MISMIP (Pattyn et al., 2012, hysteresis experiment EXP 3) and also used (modified) in other studies that conceptually investigate the stability of marine ice sheets (Goldberg et al., 2009; Gudmundsson et al., 2012). We use a piecewise cubic spline interpolation between the nodes x_c (location of the maximum of a central ridge), $\pm x_d$ (location of the minimum of a bed depression) and $\pm x_s$ (location of a coastal sill). At each of these nodes a value for the bed elevation as well as the first derivative (equal to zero, since the nodes are locations of local extrema) are prescribed. On the ocean-ward side of the sill another node with a non-zero first derivative ensures the steep sloping of the bed. The bed section between $\pm x_d$ and $\pm x_s$ is down-sloping inland and hence referred to as retrograde section in the following. Given the symmetry, the domain can be divided into two drainage basins, mirroring each other ("basin l" for the LHS of the domain, i.e. for $x < x_c$, and "basin r" for the RHS of the domain, i.e. for $x > x_c$). Retrograde bed sections can be found in several connected drainage basins of the WAIS. To illustrate this, Fig. 2 shows cross-sections through the WAIS and its underlying bed topography along three transects, each of which connects two major drainage basins. The transects do not represent flow lines of the ice but exemplify the overdeepened geometry of parts of the basins. The average slope of PIG's retrograde bed section along transect *a* (that indeed goes through the main trough of the ice stream, Figs. 1 and 2a) is comparable to the maximum slope of the retrograde section in our setup (both are in the order of -10^{-3}).

The model is set up in flow line, hence there is no variation in cross-flow direction (y direction). However, to maintain the function of the model (i.e. the finite difference scheme), which is designed for two horizontal dimensions, we use three grid cells in y direction and the lateral boundaries are periodic. A boundary condition in x direction is prescribed such that the calving front may not exceed $x = \pm 700$ km. Relevant parameter values as well as the non-linear friction law are the same as in the MISMIP3d experiments (Pattyn et al., 2013). The experiments are carried out on a fixed regular grid with a spatial resolution of $\Delta x = 1$ km and $\Delta y = 1.5$ km.

Each of the simulations presented in this study is a set of three subsequent experiments, namely spinup, perturbation and relaxation. The spinup starts from an initial block of ice with a uniform upper surface elevation of 2000 m. A symmetric ice-sheet-shelf system evolves with grounding lines located on the ocean-ward sides of the sill (Fig. 3). The system is run into equilibrium (the grounding line positions are constant and the rate of relative volume change is smaller than 10^{-7} yr after 30 kyr). The steady-state ice sheet is then perturbed locally by applying melting beneath the ice shelf only in the RHS basin r. The parameters of the melt-rate equation are chosen such that the grounding line in basin r is forced to retreat beyond the tip of the sill, being located on the retrograde section of the bed at the end of this 1.3 kyr perturbation phase. In the third and last experiment, the sub-shelf melt rates are set to 0 again (i.e. the same boundary conditions as in the spinup experiment apply) and the model is run for several 10 kyr, allowing the previously perturbed system to relax into a new steady-state. This relaxation phase is analyzed in the results section.

This sequence of experiments is carried out for a range of different elevations of the central bed ridge, i.e. the bed section between the minima of the depressions, $-x_d < x < x_d$ (compare Fig. 3a to c). To this end, the piece-wise cubic spline interpolation that defines the bed geometry between x_c and $\pm x_d$ is modified by prescribing a different value of b_c at node x_c for each individual setup. The interpolation remains unchanged otherwise, thus the bed sections for $x \leq -x_d$ and $x \geq x_d$, respectively, are smoothly connected to the modified central bed section and are identical throughout all simulations. In the following text, individual simulations are abbreviated with "BC" followed by the value of the prescribed central bed elevation, e.g. BC+200 names the simulation using a value of $b_c = +200$ m.

TCD
8, 4885–4912, 2014

3 Results

Depending on the bed geometry, we investigate three qualitatively different scenarios of the time evolution of the ice sheet after cessation of the perturbation by basal ice-shelf melting in the RHS basin r. In all three scenarios the grounding line in basin r continues to retreat after cessation of the forcing. It then migrates beyond the local minimum of the bed depression and stabilizes on the RHS flank of the central ridge.

The further evolution of the ice sheet depends on the bed topography. In the simulations with central bed elevation values ranging from $b_c = -460$ to $+330$ m the grounding line in the LHS basin l starts to retreat after a time of some kyr to several 10 kyr. The grounding line passes the tip of the local sill followed by an unstable retreat on the retrograde section of the bed. Similar to the previous retreat in basin r the grounding line then stabilizes on the LHS flank of the central ridge. The resulting steady-state ice sheet is symmetric again and has shrunken significantly compared to its initial steady-state. This scenario is referred to as “unstable” scenario U afterwards (Figs. 3 and 4a). For the simulations with $b_c \geq +340$ m the grounding line in basin l remains located on the ocean-ward side of the sill. The resulting steady-state ice sheet hence has an asymmetric shape (“stable” scenario S, Fig. 4b). Simulations using a central bed elevation of $b_c \leq -470$ m initially show the same process of unstable grounding line retreat in basin l as in scenario U. However, in contrast to scenario U, the grounding line in basin l does not stabilize and at some point a grounding line retreat in basin r sets in again. This results in a total collapse of the ice sheet (“collapsing” scenario C). We visualize the time evolution of the ice-sheet profile also in a short movie for the scenarios U and S, respectively (see Supplement).

Characteristic features that go along with the triggered unstable grounding line retreat in the RHS basin r are a shift of the ice divide position (defined as the location through which there is zero ice flux) towards the LHS basin l, a non-zero and increasing ice flux through x_c (from basin l into basin r) and a decrease in grounded ice sheet volume (Figs. 5–7). The simulations of the unstable scenario U imply a triggered MISI

TCD
8, 4885–4912, 2014

also in basin l, causing the ice divide to shift back to its original position, including a further decrease in ice sheet volume. Before stabilization, a slight grounding line retreat in basin r sets in again (Fig. 5a). In the stable scenario S the position of the ice divide, the ice flux through x_c and the ice volume adjust only slightly after the grounding line in basin r has stabilized, reflecting the asymmetric shape of the resulting ice sheet (Figs. 4b and 6). The collapsing scenario C is very similar to scenario U with the difference that in the former the reoccurrence of grounding line retreat in basin r is significantly larger with grounded ice volume dropping to zero eventually as both grounding lines synchronously reach $x = 0$ (Fig. 7).

3.1 Scaling of symmetric steady-state ice sheets

For several simplified ice-sheet problems analytic solutions of steady-state ice-sheet profiles have been derived (Greve and Blatter, 2009; Bueler, 2014). Vialov (1958) derived an analytic solution for the profile of a symmetric, isothermal steady-state flow-line ice sheet for the SIA of the momentum balance, where vertical shearing is dominant. The surface elevation h of the ice sheet that is grounded on a flat bed is then basically determined by its length L:

$$h(x) = h_c \cdot \left[1 - \left(\frac{x}{L}\right)^{(n+1)/n}\right]^{n/(2n+2)} \quad \text{with} \quad x \in [-L, L], \tag{1}$$

where

$$h_c = 2^{n/(2n+2)} \cdot \left(\frac{a}{A}\right)^{1/(2n+2)} \cdot L^{1/2} \tag{2}$$

is the surface elevation at the center of the ice sheet (at the ice divide) with uniform accumulation a and ice softness A. The equation in brackets in Eq. (1) represents the non-dimensionalized universal shape of an SIA-ice sheet under the above conditions.

Vialov's and our idealized cases share several assumptions but also differ substantially in some respects. In contrast to Vialov, we use a non-flat bed, allow for basal

TCD
8, 4885–4912, 2014

sliding and longitudinal stresses in the ice sheet are predominant over vertical shearing (the SSA-velocities are large compared to the SIA-velocities for the major part of the grounded ice sheet), features which are typical for ice streams found in the WAIS. However, using Eq. (1) with $n = 3$ and prescribing h_c and L from model output, the Vialov profile (dotted lines in Fig. 3b and c) resembles the profile that we obtain from our simulation (solid gray lines in Fig. 3b and c).

For a given bed topography in our simulations of scenario U the initial and final symmetric steady-state profiles of the ice sheet substantially differ in size but have a similar shape. Equation (1) can be used to scale between two such ice sheets of lengths L_0 and L_1, respectively,

$$h_1(x_1) = h_0(x) \cdot \left(\frac{L_1}{L_0}\right)^{1/2}, \quad \text{where} \quad x_1 = x \cdot \frac{L_1}{L_0} \quad \text{with} \quad x \in [-L_0, L_0], \tag{3}$$

using the same scaling exponent of 1/2 as derived for the central ice-thickness of the Vialov profile. We apply the above scaling using the initial surface elevation h_0 as well as the initial and final grounding line positions from model output to arrive at the final surface elevation h_1 (shown exemplary for two different central ridge elevations as dashed lines in Fig. 4b and c). That is to say, the simulated ice sheet exhibits more or less the same relation between its central ice thickness and its horizontal extent.

3.2 Scaling of transition time between instabilities

In the unstable scenario U two MISIs succeed each other. The first MISI in the RHS basin r (which was previously triggered by a local perturbation) causes the initiation of a second MISI in the connected LHS basin l, a process going on only due to internal ice sheet dynamics. The transition time Δt between the occurrence of both events of unstable grounding line retreat (Fig. 5a) ranges from several kyr to 10 kyr and is practically independent of the initial trigger. Assuming that the difference between the ice thickness of the two states is the internal force for the transition, we scale Δt with

TCD
8, 4885–4912, 2014

$\Delta H_c = (h_1 - h_0)(x = 0)$, i.e. the central ice thickness difference between the final and initial steady-states of the ice sheet (Fig. 3a). The relation

$$\Delta t = \Delta t_{\min} + C \cdot (\Delta H_c - \Delta H_{c,\min})^{-1} \quad (4)$$

provides a good approximation of the transition time (Fig. 8). Here the constants $\Delta t_{\min}$ and $\Delta H_{c,\min}$ have clear physical interpretations and represent a minimum transition time and a minimum ice thickness difference, respectively (Fig. 8). These asymptotes constrain the regime for which the MISI in basin I is triggered and the final steady-state ice sheet is of symmetric shape (scenario U): for $\Delta H_c < \Delta H_{c,\min}$ the ice sheet remains asymmetric (scenario S) whereas in the regime $\Delta t < \Delta t_{\min}$ it collapses completely (scenario C).

Replacing ΔH_c with the above definition and using Eq. (3), the transition time (Eq. 4) can be rewritten as

$$\Delta t = \Delta t_{\min} + C \cdot \left(h_{0,c} \cdot \left[\left(\frac{L_1}{L_0} \right)^{1/2} - 1 \right] - \Delta H_{c,\min} \right)^{-1}, \quad (5)$$

which allows a scaling of the transition time based on the initial central surface elevation of the ice sheet, $h_{0,c}$, and Vialov's $L^{1/2}$-dependency.

The transition time can also be expressed in terms of the grounding line shift between the ice sheet's two steady-states $\Delta L = L_0 - L_1$. Since ΔL is a linear function of the central ice thickness difference ΔH_c, Eq. (4) can also be written as

$$\Delta t = \Delta t_{\min} + D \cdot (\Delta L - \Delta L_{\min})^{-1} \quad (6)$$

by using a different coefficient D instead of C. The threshold $\Delta H_{c,\min}$ is replaced by a threshold of a minimum grounding line retreat, $\Delta L_{\min}$, which has to be exceeded to enable the MISI initiation in basin I.

TCD
8, 4885–4912, 2014

3.3 Transient dynamic thinning and basin-stability

Here we describe the temporal evolution of the ice sheet after cessation of its perturbation in detail. We reveal the origin of the qualitative difference between the unstable/collapsing scenarios U/C, which imply a MISI transition between basin l and r, and the stable scenario S, which does not imply such a transition. The grounding line retreat in the RHS basin r, which continues after the perturbation, is associated with a dynamic thinning of the upstream ice (Figs. 9 and 10). The thinning declines with increasing distance from the grounding line towards the interior of the domain but is still non-zero in the center of the ice sheet and reaches further into the LHS basin l with time. While the grounding line stabilizes in basin r and the local thinning rate goes to zero, the inland thinning propagates far enough into basin l to reach the local grounding line. Here the increasing thinning rate eventually results in a grounding line retreat. Depending on the scenario, the thinning in basin l then continues to propagate back into the interior of the basin (scenarios U and C, instability in basin l triggered) or ceases (scenario S, instability not triggered).

We compare the time evolution of the ice in basin l for two simulations which show this qualitative difference in stability while having almost the same bed topography (simulations BC+330 and BC+340). In simulation BC+330 the grounding line in basin l retreats beyond the point of maximum sill elevation. The thinning continues to propagate into the interior and the thinning rate increases during the grounding line's unstable retreat on the retrograde section of the bed. Temporarily, basin r is now affected by an inland thinning, which results in a slight retreat of the previously stabilized grounding line in basin r (Fig. 9). The rate of the thinning in both basins goes to zero as the grounding lines find their steady-state position synchronously. In simulation BC+340, the thinning rate in basin l goes to zero as the grounding line migrates upstream towards the point of local maximum bed elevation (Fig. 10c). The cumulative thinning there (at the tip of the sill) is insufficient to cause the ice to become afloat (indicated by dotted cross in Fig. 10b). Due to the almost identical setups of both simulations we identify the location of maximum elevation of the sill in basin l as the instability threshold, i.e. a grounding line retreat beyond this point implies the initiation of a MISI in basin l.

4 Discussion and conclusions

We investigate the possibility of whether a MISI can be triggered from the direction of the ice divide as opposed to coastal forcing and to this end study the interaction between connected basins. In our experiments we perturb one basin to analyze its interaction with a connected basin. The extent of grounding line retreat in the aftermath of the triggered MISI in the perturbed basin significantly determines the degree of interaction with the other basin, including a scenario of an induced MISI (scenarios U and C).

The transition of the MISI between the two basins takes place without external forcing and hence only due to internal ice sheet dynamics. This feature is robust against a reduction in surface accumulation (simulations using an accumulation rate one order of magnitude lower demonstrate the same quality like the runs shown here). While the unstable grounding line retreat in our experiments is in accordance with findings by Schoof (2007), the possibility of a MISI in three dimensions highly depends on the geometry of the ice sheet and the underlying bed (Joughin et al., 2010; Katz and Worster, 2010; Gudmundsson, 2013; Parizek et al., 2013; Mengel and Levermann, 2014; Joughin et al., 2014). The time scales of ice sheet response in our experiments are in the order of magnitude of 1 kyr (unstable grounding line retreat) to 10 kyr (transition time between MISIs in basin l and r). The stabilizing effect of buttressing in three dimensions would most probably slow down basin interaction.

The underlying mechanism of basin interaction in our simulations is based on a dynamic thinning of the ice (Fig. 4). Originating in one basin and reaching as far as to the grounding line of the other basin, it enables far field communication between the grounding lines of both basins (Figs. 9 and 10). Dynamic thinning is of course not limited to two dimensions. However, in three dimensions it might propagate less straight away from the grounding line but also spread laterally. Nevertheless, a possible influence of future thinning in the basins of the Amundsen Sea Sector onto other basins in the WAIS, e.g. extensive thinning of PIG affecting FRIS basin, cannot be excluded.

Based on the Vialov profile (Eq. 1) we do a simple scaling of the initial and final symmetric steady-state surface elevations of the grounded ice sheet for the unstable scenario U. The Vialov profile was derived using several assumptions which don't apply to our setup. In particular it is an SIA-solution for a flat, non-sliding bed, while our simulations are SSA-dominated, our bed topography is non-trivial and we allow for basal sliding. Given these substantial differences, the ice sheet profiles from Vialov's equation and from our model results are in good agreement and also the scaling of steady-state surface elevations via Eq. (3) works reasonably well.

The elevation of the central bed ridge in our setup has a strong influence on the steady-state grounding line position in the RHS basin r (Fig. 3). With increasing elevation of the central ridge the grounding line stabilizes farther from the center with the result that far field thinning in the LHS basin l becomes weaker and thus takes longer to affect the grounding line in basin l (Fig. 8). This also becomes apparent from Eq. (6), which states that the transition time scales inversely with the extent of grounding line retreat and includes a threshold of a minimum grounding line retreat below which basin l remains stable. The central ridge may hence be considered as a barrier which can dampen/facilitate basin interaction when being elevated/lowered. In other words, grounding line retreat in the perturbed basin strongly determines the degree and the quality of the interaction with the connected basin.

The Supplement related to this article is available online at doi:10.5194/tcd-8-4885-2014-supplement.

Acknowledgements. J. Feldmann is funded by Deutsche Bundesstiftung Umwelt.

References

Anandakrishnan, S., Alley, R. B., and Waddington, E. D.: Sensitivity of the ice-divide position in Greenland to climate change, Geophys. Res. Lett., 21, 441–444, doi:10.1029/94GL00094, 1994. 4887

Beckmann, A. and Goosse, H.: A parameterization of ice shelf–ocean interaction for climate models, Ocean Model., 5, 157–170, doi:10.1016/S1463-5003(02)00019-7, 2003. 4888

Bindschadler, R. A., Nowicki, S., Abe-ouchi, A., Aschwanden, A., Choi, H., Fastook, J., Granzow, G., Greve, R., Gutowski, G., Herzfeld, U., Jackson, C., Johnson, J., Khroulev, C., Levermann, A., Lipscomb, W. H., Martin, M. A., Morlighem, M., Parizek, B. R., Pollard, D., Price, S. F., Ren, D., Saito, F., Sato, T., Seddik, H., Seroussi, H., Takahashi, K., Walker, R., and Wang, W. L.: Ice-sheet model sensitivities to environmental forcing and their use in projecting future sea level (the SeaRISE project), J. Glaciol., 59, 195–224, doi:10.3189/2013JoG12J125, 2013. 4887

Bueler, E.: An exact solution for a steady, flow-line marine ice sheet, J. Glaciol., accepted, 2014. 4892

Bueler, E. and Brown, J.: Shallow shelf approximation as a “sliding law” in a thermomechanically coupled ice sheet model, J. Geophys. Res., 114, 1–21, doi:10.1029/2008JF001179, 2009. 4888

Cuffey, K. M. and Clow, G. D.: Temperature, accumulation, and ice sheet elevation in central Greenland through the last deglacial transition, J. Geophys. Res., 102, 26383–26396, doi:10.1029/96JC03981, 1997. 4887

Favier, L., Durand, G., Cornford, S. L., Gudmundsson, G. H., Gagliardini, O., Gillet-Chaulet, F., Zwinger, T., Payne, A. J., and Le Brocq, A. M.: Retreat of Pine Island Glacier controlled by marine ice-sheet instability, Nature Climate Change, 5, 1–5, doi:10.1038/nclimate2094, 2014. 4886

Feldmann, J., Albrecht, T., Khroulev, C., Pattyn, F., and Levermann, A.: Resolution-dependent performance of grounding line motion in a shallow model compared with a full-Stokes model according to the MISMIP3d intercomparison, J. Glaciol., 60, 353–360, doi:10.3189/2014JoG13J093, 2014. 4888

Goldberg, D., Holland, D. M., and Schoof, C.: Grounding line movement and ice shelf buttressing in marine ice sheets, J. Geophys. Res., 114, F04026, doi:10.1029/2008JF001227, 2009. 4889

Greve, R. and Blatter, H.: Dynamics of ice sheets and glaciers, Chapter no. 1, in: Advances in Geophysical and Environmental Mechanics and Mathematics, Springer, Berlin, Heidelberg, doi:10.1007/978-3-642-03415-2, 2009. 4892

Gudmundsson, G. H.: Ice-shelf buttressing and the stability of marine ice sheets, The Cryosphere, 7, 647–655, doi:10.5194/tc-7-647-2013, 2013. 4896

Gudmundsson, G. H., Krug, J., Durand, G., Favier, L., and Gagliardini, O.: The stability of grounding lines on retrograde slopes, The Cryosphere, 6, 1497–1505, doi:10.5194/tc-6-1497-2012, 2012. 4889

Holt, J. W., Blankenship, D. D., Morse, D. L., Young, D. A., Peters, M. E., Kempf, S. D., Richter, T. G., Vaughan, D. G., and Corr, H. F. J.: New boundary conditions for the West Antarctic ice sheet: subglacial topography of the Thwaites and Smith glacier catchments, Geophys. Res. Lett., 33, L09502, doi:10.1029/2005GL025561, 2006. 4887

Jacobs, S. S., Jenkins, A., Giulivi, C. F., and Dutrieux, P.: Stronger ocean circulation and increased melting under Pine Island Glacier ice shelf, Nat. Geosci., 4, 519–523, doi:10.1038/ngeo1188, 2011. 4887

Joughin, I. and Alley, R. B.: Stability of the West Antarctic ice sheet in a warming world, Nat. Geosci., 4, 506–513, doi:10.1038/ngeo1194, 2011. 4886

Joughin, I., Smith, B. E., and Holland, D. M.: Sensitivity of 21st century sea level to ocean-induced thinning of Pine Island Glacier, Antarctica, Geophys. Res. Lett., 37, L20502, doi:10.1029/2010GL044819, 2010. 4896

Joughin, I., Smith, B. E., and Medley, B.: Marine ice sheet collapse potentially under way for the Thwaites Glacier Basin, West Antarctica, Science, 344, 735–738, doi:10.1126/science.1249055, 2014. 4886, 4896

Katz, R. F. and Worster, M. G.: Stability of ice-sheet grounding lines, P. Roy. Soc. A-Math. Phy., 466, 1597–1620, doi:10.1098/rspa.2009.0434, 2010. 4886, 4896

Martin, M. A., Winkelmann, R., Haseloff, M., Albrecht, T., Bueler, E., Khroulev, C., and Levermann, A.: The Potsdam Parallel Ice Sheet Model (PISM-PIK) – Part 2: Dynamic equilibrium simulation of the Antarctic ice sheet, The Cryosphere, 5, 727–740, doi:10.5194/tc-5-727-2011, 2011. 4888

Medley, B., Joughin, I., Smith, B. E., Das, S. B., Steig, E. J., Conway, H., Gogineni, S., Lewis, C., Criscitiello, A. S., McConnell, J. R., van den Broeke, M. R., Lenaerts, J. T. M., Bromwich, D. H., Nicolas, J. P., and Leuschen, C.: Constraining the recent mass balance of Pine Island and Thwaites glaciers, West Antarctica, with airborne observations of snow accumulation, The Cryosphere, 8, 1375–1392, doi:10.5194/tc-8-1375-2014, 2014. 4887

Mengel, M. and Levermann, A.: Ice plug prevents irreversible discharge from East Antarctica, Nature Climate Change, 4, 451–455, doi:10.1038/NCLIMATE2226, 2014. 4896

Mercer, J. H.: West Antarctic ice sheet and CO_2 greenhouse effect: a threat of disaster, Nature, 271, 321–325, 1978. 4886

Mouginot, J., Rignot, E., and Scheuchl, B.: Sustained increase in ice discharge from the Amundsen Sea Embayment, West Antarctica, from 1973 to 2013, Geophys. Res., 41, 1576–1584, doi:10.1002/2013GL059069, 2014. 4887

Nereson, N. and Raymond, C.: The elevation history of ice streams and the spatial accumulation pattern along the Siple Coast of West Antarctica inferred from ground-based radar data from three inter-ice-stream ridges, J. Glaciol., 47, 303–313, doi:10.3189/172756501781832197, 2001. 4887

Nereson, N., Hindmarsh, R., and Raymond, C.: Sensitivity of the divide position at Siple Dotne, West Antarctica, to boundary forcing, Ann. Glaciol., 27, 207–214, 1998. 4887

Parizek, B. R., Christianson, K., Anandakrishnan, S., Alley, R. B., Walker, R. T., Edwards, R. A., Wolfe, D. S., Bertini, G. T., Rinehart, S. K., Bindschadler, R. A., and Nowicki, S. M. J.: Dynamic (in)stability of Thwaites Glacier, West Antarctica, J. Geophys. Res.-Earth, 118, 638–655, doi:10.1002/jgrf.20044, 2013. 4896

Park, J. W., Gourmelen, N., Shepherd, A., Kim, S. W., Vaughan, D. G., and Wingham, D. J.: Sustained retreat of the Pine Island Glacier, Geophys. Res. Lett., 40, 2137–2142, doi:10.1002/grl.50379, 2013. 4887

Pattyn, F., Schoof, C., Perichon, L., Hindmarsh, R. C. A., Bueler, E., de Fleurian, B., Durand, G., Gagliardini, O., Gladstone, R., Goldberg, D., Gudmundsson, G. H., Huybrechts, P., Lee, V., Nick, F. M., Payne, A. J., Pollard, D., Rybak, O., Saito, F., and Vieli, A.: Results of the Marine Ice Sheet Model Intercomparison Project, MISMIP, The Cryosphere, 6, 573–588, doi:10.5194/tc-6-573-2012, 2012. 4889

Pattyn, F., Perichon, L., Durand, G., Favier, L., Gagliardini, O., Hindmarsh, R. C., Zwinger, T., Albrecht, T., Cornford, S., Docquier, D., Fürst, J. J., Goldberg, D., Gudmundsson, G. H., Humbert, A., Hütten, M., Huybrechts, P., Jouvet, G., Kleiner, T., Larour, E., Martin, D., Morlighem, M., Payne, A. J., Pollard, D., Rückamp, M., Rybak, O., Seroussi, H., Thoma, M., and Wilkens, N.: Grounding-line migration in plan-view marine ice-sheet

models: results of the ice2sea MISMIP3d intercomparison, J. Glaciol., 59, 410–422, doi:10.3189/2013JoG12J129, 2013. 4888, 4890
Pritchard, H. D., Ligtenberg, S. R. M., Fricker, H. A., Vaughan, D. G., van den Broeke, M. R., and Padman, L.: Antarctic ice-sheet loss driven by basal melting of ice shelves., Nature, 484, 502–5, doi:10.1038/nature10968, 2012. 4887
Rignot, E. and Mouginot, J.: Widespread, rapid grounding line retreat of Pine Island, Thwaites, Smith, and Kohler glaciers, West Antarctica, from 1992 to 2011, Geophys. Res. Lett., 41, 3502–3509, doi:10.1002/2014GL060140, 2014. 4887
Rignot, E., Bamber, J. L., den Broeke, M. R. V., Li, Y., Davis, C., de Berg, W. J. V., and Meijgaard, E.: Recent Antarctic ice mass loss from radar interferometry and regional climate modelling, Nat. Geosci., 1, 106–110, 2008. 4887
Rignot, E., Jacobs, S., Mouginot, J., and Scheuchl, B.: Ice-shelf melting around Antarctica, Science, 341, 266–270, doi:10.1126/science.1235798, 2013. 4887
Schoof, C.: Ice sheet grounding line dynamics: Steady states, stability, and hysteresis, J. Geophys. Res., 112, F03S28, doi:10.1029/2006JF000664, 2007. 4886, 4889, 4896
Shepherd, A., Wingham, D. J., and Mansley, J. A. D.: Inland thinning of the Amundsen Sea sector, West Antarctica, October, 29, 7–10, 2002. 4887
Stuiver, M., Denton, G. H., Hughes, T. J., and Fastook, J. L.: History of the Marine Ice Sheet in West Antarctica During the Last Glaciation: a Working Hypothesis, in: The Last Great Ice Sheets, edited by: Denton, G. H. and Hughes, T. J., 319–436, John Wiley and Sons, New York, 1981. 4887
Tinto, K. J. and Bell, R. E.: Progressive unpinning of Thwaites Glacier from newly identified offshore ridge: constraints from aerogravity, Geophys. Res. Lett., 38, 1–6, doi:10.1029/2011GL049026, 2011. 4887
Vaughan, D. G., Corr, H. F. J., Ferraccioli, F., Frearson, N., O'Hare, A., Mach, D., Holt, J. W., Blankenship, D. D., Morse, D. L., and Young, D. A.: New boundary conditions for the West Antarctic ice sheet: subglacial topography beneath Pine Island Glacier, Geophys. Res. Lett., 33, L09501, doi:10.1029/2005GL025588, 2006. 4887
Vialov, S. S.: Regularities of glacial shields movement and the theory of plastic viscous flow, Physics of the Movements of Ice IAHS, 47, 266–275, 1958. 4892
Walker, D. P., Brandon, M. A., Jenkins, A., Allen, J. T., Dowdeswell, J. A., and Evans, J.: Oceanic heat transport onto the Amundsen Sea shelf through a submarine glacial trough, Geophys. Res. Lett., 34, L02602, doi:10.1029/2006GL028154, 2007. 4887

TCD
8, 4885–4912, 2014

J. Feldmann and A. Levermann

Title Page
Abstract | Introduction
Conclusions | References
Tables | Figures
◀I | ▶I
◀ | ▶
Back | Close
Full Screen / Esc
Printer-friendly Version
Interactive Discussion

Winkelmann, R., Martin, M. A., Haseloff, M., Albrecht, T., Bueler, E., Khroulev, C., and Levermann, A.: The Potsdam Parallel Ice Sheet Model (PISM-PIK) – Part 1: Model description, The Cryosphere, 5, 715–726, doi:10.5194/tc-5-715-2011, 2011. 4888

TCD

8, 4885–4912, 2014

Interaction of marine ice-sheet instabilities in two drainage basins

J. Feldmann and A. Levermann

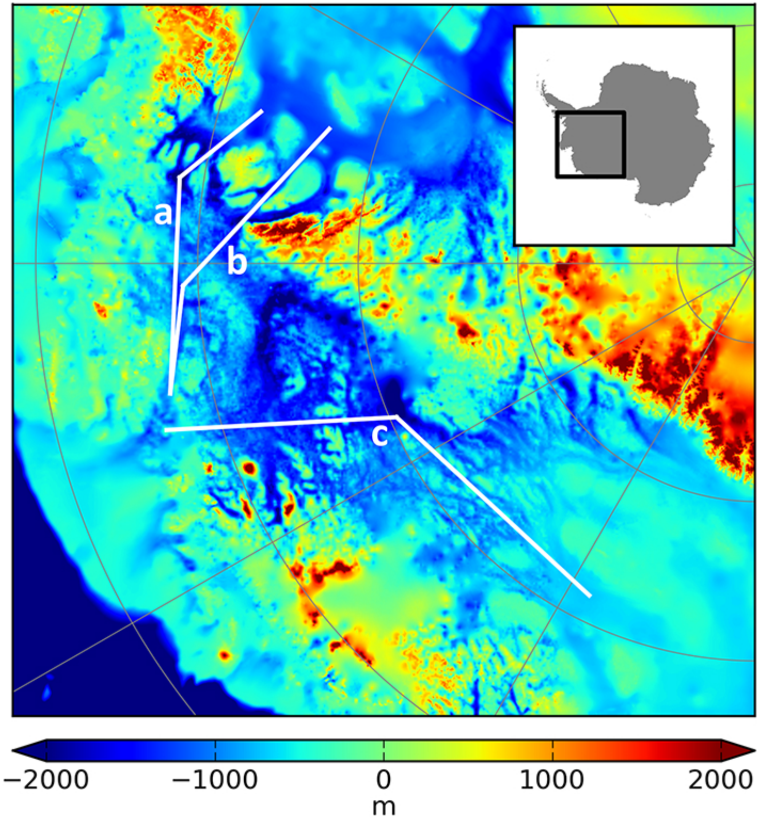

Figure 1. Topographic map of the bedrock underlying the Antarctic Ice Sheet. Each of the transects (white lines) connects two major drainage basins of the WAIS. The bed topography and the ice profile along transects a, b and c are shown in the corresponding panels of Fig. 2.

TCD
8, 4885–4912, 2014

Interaction of marine ice-sheet instabilities in two drainage basins

J. Feldmann and A. Levermann

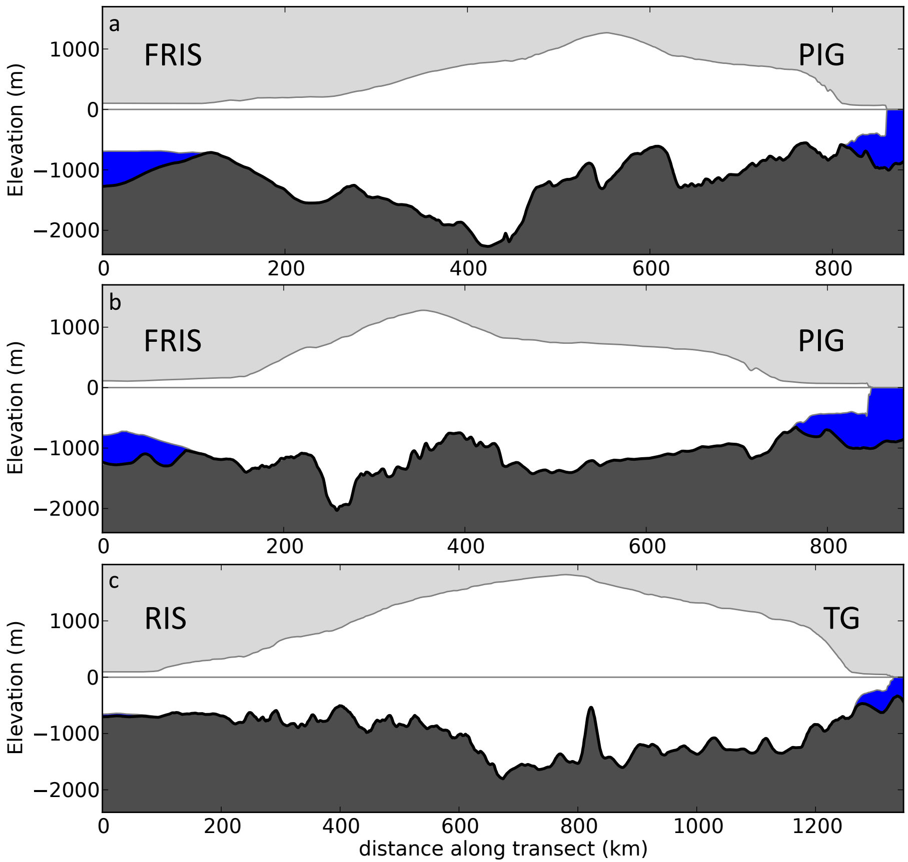

Figure 2. Cross-sections through the ice and the bed along the transects depicted in Fig. 1: bed topography (dark gray), ice sheet (white), ocean (blue). Both transects **(a)** and **(b)** connect the basins of Filchner–Ronne Ice Shelf (FRIS) and Pine Island Glacier (PIG). Transect **(c)** goes through the basins of Ross Ice Shelf (RIS) and Thwaites Glacier (TG).

TCD
8, 4885–4912, 2014

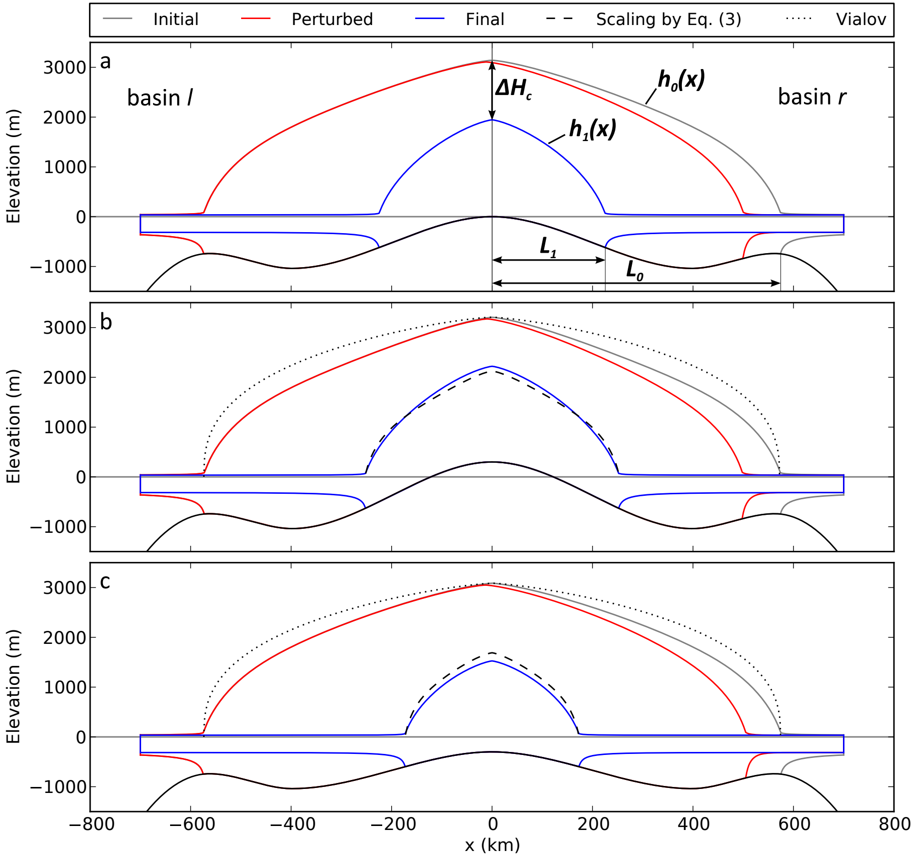

Figure 3. Ice sheet profiles at three stages of simulation for three different values of central bed elevation **(a)** $b_c = 0$ m, **(b)** $b_c = +300$ m and **(c)** $b_c = -300$ m. Panel **(b)** depicts the notation used in the text.

TCD
8, 4885–4912, 2014

Interaction of marine ice-sheet instabilities in two drainage basins

J. Feldmann and A. Levermann

TCD
8, 4885–4912, 2014

Interaction of marine ice-sheet instabilities in two drainage basins

J. Feldmann and A. Levermann

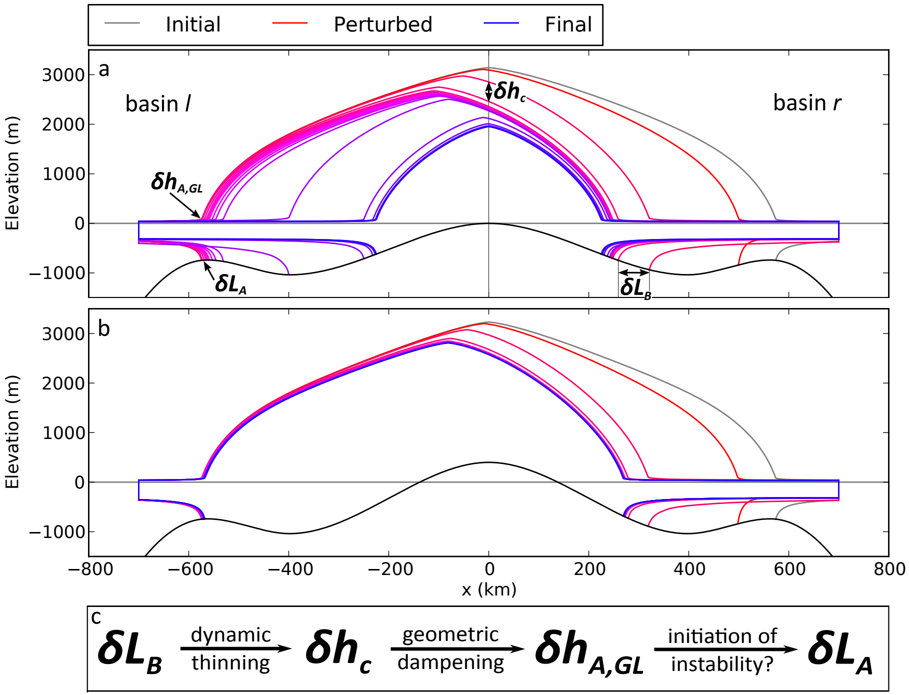

Figure 4. Profiles of the transient ice sheet between the end of perturbation (red) and the final steady-state (blue) for two different values of central bed elevation **(a)** $b_c = 0$ m (example of unstable scenario U, same as in Fig. 3a) and **(b)** $b_c = +400$ m (example of stable scenario S). The time interval between two consecutive profiles is 1 kyr. The bottom panel explains the mechanism of basin interaction conceptually with the notation depicted in panel **(a)**.

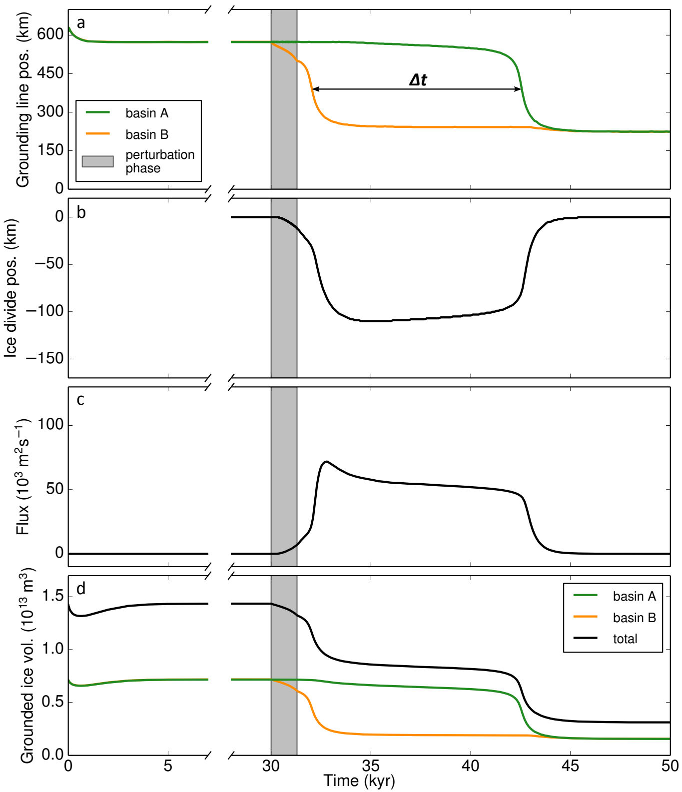

Figure 5. Timeseries for the unstable scenario U (simulation BC0, see Figs. 2a and 3a) of **(a)** the absolute value of the grounding line positions **(b)** the position of the ice divide (as defined in the text), **(c)** the flux through $x = 0$ (positive in x direction) and **(d)** the grounded ice volume. The transition time Δt, used in Eqs. (4)–(6), is depicted by a double-headed arrow in panel **(a)**.

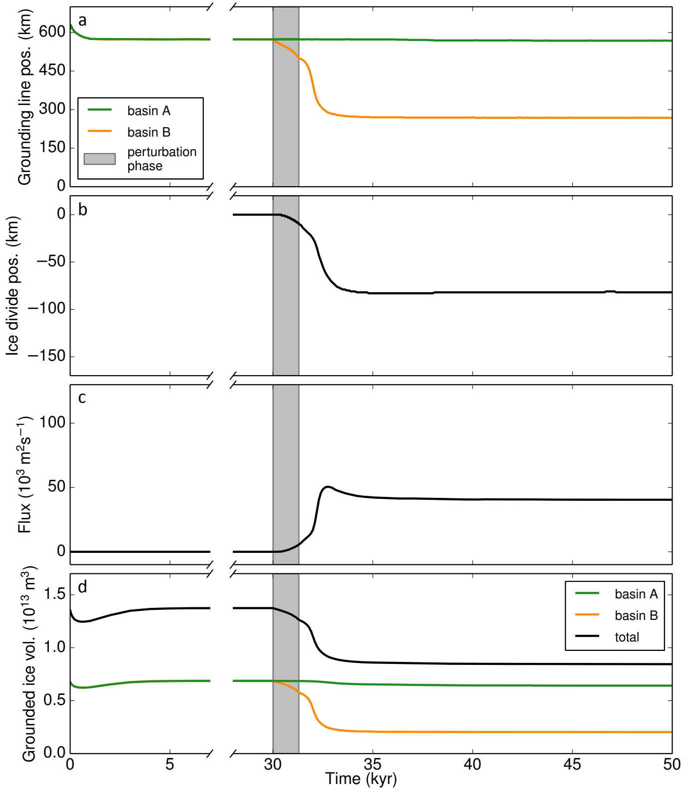

Figure 6. Same as Fig. 5 but here for the stable scenario S (simulation BC+400, see Fig. 4b).

TCD
8, 4885–4912, 2014

Interaction of marine ice-sheet instabilities in two drainage basins

J. Feldmann and A. Levermann

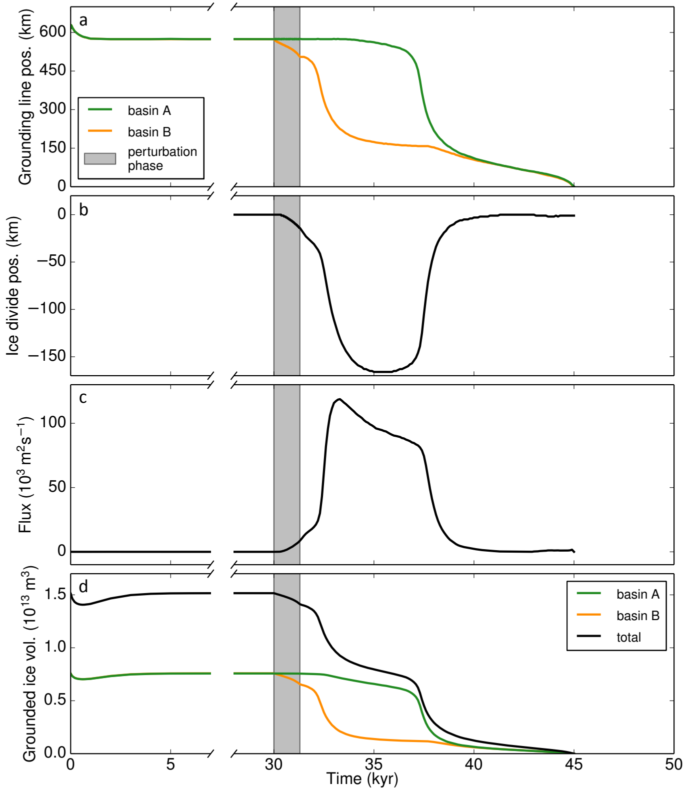

Figure 7. Same as Fig. 5 but here for the collapsing scenario C (simulation BC-500).

TCD
8, 4885–4912, 2014

Interaction of marine ice-sheet instabilities in two drainage basins

J. Feldmann and A. Levermann

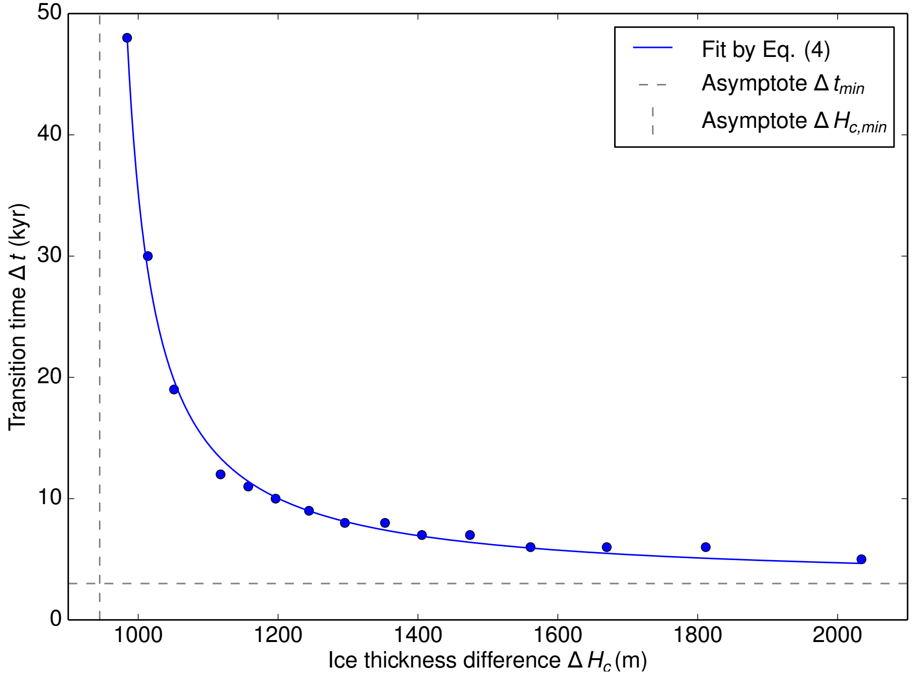

Figure 8. Transition time of MISI Δt plotted against central ice thickness difference between initial and final steady states of the ice sheet ΔH_c. Each dot represents a simulation of scenario U with a different central bed elevation b_c.

TCD
8, 4885–4912, 2014

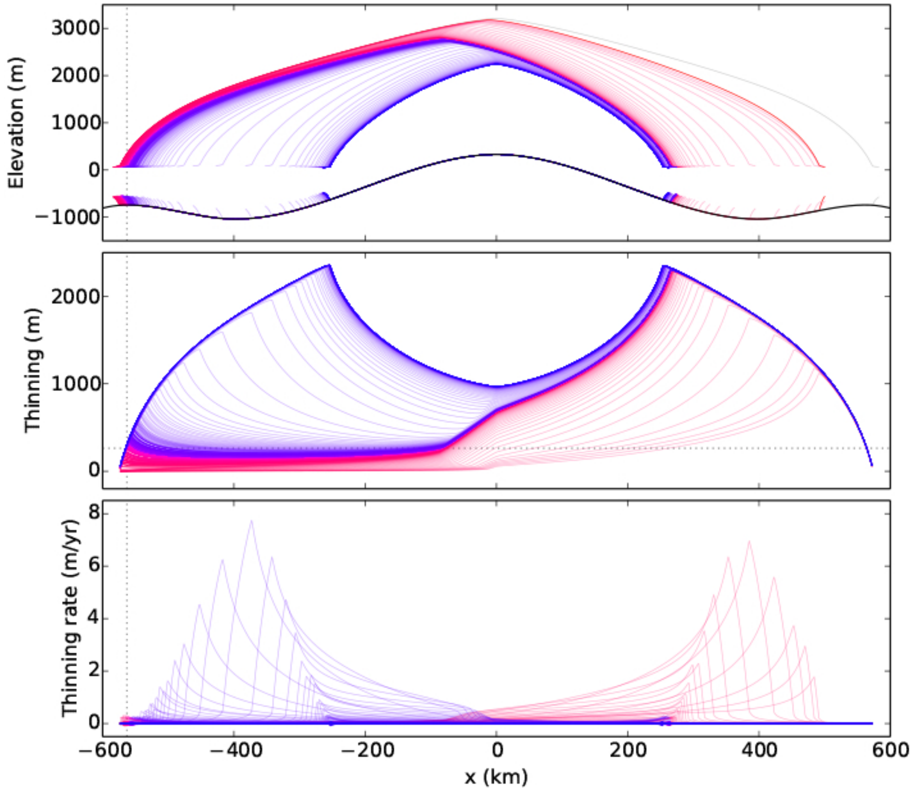

Figure 9. Ice sheet **(a)** profile, **(b)** thinning with respect to the ice thickness at the end of perturbation and **(c)** tinning rate at multiple stages (time interval 100 yr) of the unstable scenario U (simulation BC+330). The ice shelf is truncated for better visibility. The vertical dotted line indicates the location of maximum sill elevation. The horizontal dotted line in panel **(b)** gives the amount of cumulative thinning necessary to cause the ice situated on the local bed maximum to become afloat. The same color-coding as in Fig. 4 applies.

TCD
8, 4885–4912, 2014

Interaction of marine ice-sheet instabilities in two drainage basins

J. Feldmann and A. Levermann

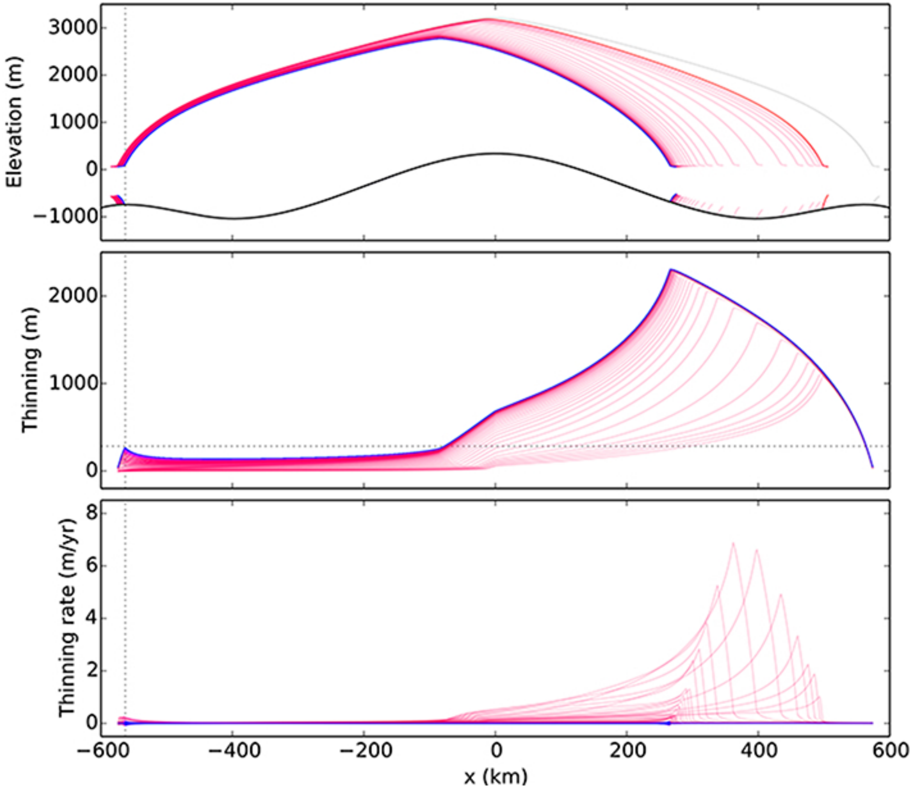

Figure 10. Same as Fig. 9 but here for the stable scenario S (simulation BC+340).

TCD
8, 4885–4912, 2014

Interaction of marine ice-sheet instabilities in two drainage basins

J. Feldmann and A. Levermann